AGU PUBLICATIONS

Geochemistry, Geophysics, Geosystems

RESEARCH ARTICLE
10.1002/2016GC006584

Special Section:
The Arctic: An AGU Joint Special Collection

This article is a companion to *Ruppel et al.* [2016], doi:10.1002/2016GC006582.

Key Points:
- Spatially extensive and dense velocity analyses are used to map subsea permafrost distribution on the U.S. Beaufort continental shelf
- This study provides margin-scale evidence that continuous subsea IBPF does not currently extend to the edge of the continental shelf
- U.S. Beaufort subsea permafrost has degraded substantially and the shelf-edge should be dismissed as the presumed extent of continuous IBPF

Supporting Information:
- Supporting Information S1

Correspondence to:
L. L. Brothers,
lbrothers@usgs.gov

Citation:
Brothers, L. L., B. M. Herman, P. E. Hart, and C. D. Ruppel (2016), Subsea ice-bearing permafrost on the U.S. Beaufort Margin: 1. Minimum seaward extent defined from multichannel seismic reflection data, *Geochem. Geophys. Geosyst.*, *17*, 4354–4365, doi:10.1002/2016GC006584.

Received 8 AUG 2016
Accepted 5 OCT 2016
Accepted article online 11 OCT 2016
Published online 4 NOV 2016

Subsea ice-bearing permafrost on the U.S. Beaufort Margin: 1. Minimum seaward extent defined from multichannel seismic reflection data

Laura L. Brothers[1], Bruce M. Herman[2], Patrick E. Hart[3], and Carolyn D. Ruppel[1]

[1]U.S. Geological Survey, Woods Hole, Massachusetts, USA, [2]Bureau of Ocean Energy Management, Anchorage, Alaska, USA, [3]U.S. Geological Survey, Santa Cruz, California, USA

Abstract Subsea ice-bearing permafrost (IBPF) and associated gas hydrate in the Arctic have been subject to a warming climate and saline intrusion since the last transgression at the end of the Pleistocene. The consequent degradation of IBPF is potentially associated with significant degassing of dissociating gas hydrate deposits. Previous studies interpreted the distribution of subsea permafrost on the U.S. Beaufort continental shelf based on geographically sparse data sets and modeling of expected thermal history. The most cited work projects subsea permafrost to the shelf edge (~100 m isobath). This study uses a compilation of stacking velocity analyses from ~100,000 line-km of industry-collected multichannel seismic reflection data acquired over 57,000 km^2 of the U.S. Beaufort shelf to delineate continuous subsea IBPF. Gridded average velocities of the uppermost 750 ms two-way travel time range from 1475 to 3110 m s^{-1}. The monotonic, cross-shore pattern in velocity distribution suggests that the seaward extent of continuous IBPF is within 37 km of the modern shoreline at water depths < 25 m. These interpretations corroborate recent Beaufort seismic refraction studies and provide the best, margin-scale evidence that continuous subsea IBPF does not currently extend to the northern limits of the continental shelf.

1. Introduction

Since the Pliocene, conditions conducive for permafrost and gas hydrate formation have existed in the U.S. Arctic [*Brigham and Miller*, 1984; *Collett and Dallimore*, 2003; *Lewis and Collett*, 2013; *Osterkamp and Gosink*, 1991]. Following the glacial maximum (~19 ka), global eustatic sea-level rise on the order of 120 m inundated the Beaufort continental shelf [*Bard and Fairbanks*, 1990], increasing the average annual temperature of the formerly exposed land surface from −15°C to approximately −1°C [*Brigham and Miller*, 1984; *Taylor et al*., 2013; *Weingartner et al*., 2005]. Along the U.S. Beaufort Sea continental shelf, gas hydrate may occur beneath or within subsea permafrost where it is preserved on the shelf [*Collett et al*., 2011; *Kvenvolden and Grantz*, 1990]. Of all the types of gas hydrate occurrences, these shelf, permafrost-associated gas hydrates are among the most susceptible to dissociation related to changes in climate [*Ruppel*, 2011].

In the Beaufort Sea and along most of the Arctic Ocean, the edge of the continental shelf (~100 m isobath) is conventionally proposed as the seaward limit of subsea permafrost [*Brown et al*., 1997; *Heginbottom et al*., 1993]. However, recent studies in the U.S. Beaufort and South Kara Sea shelves suggest that the shelf edge is an overestimation of the seaward extent of continuous subsea ice-bearing permafrost (IBPF) and that subsea IBPF degradation has been more extreme than previously estimated in some locations [*Brothers et al*., 2012; *Portnov et al*., 2013]. This study presents U.S. Beaufort continuous subsea IBPF distribution interpreted from velocity analyses conducted on ~100,000 line-km of petroleum industry-collected multichannel seismic (MCS) reflection data (Figures 1 and 2). Spanning the entire shelf, the seismic data provide the most spatially extensive and dense set of observations regarding IBPF so far presented for any circum-arctic shelf.

2. Permafrost Setting and Previous Studies

Permafrost is defined as ground that is at or below 0°C for 2 years or more. The term ice-bearing permafrost (IBPF) refers to soil or rock that contains, or is interpreted to contain, ice that can be detected without the aid of temperature data [*Collett et al*., 1988; *National Snow & Ice Data Center*, 2016]. Conditions where

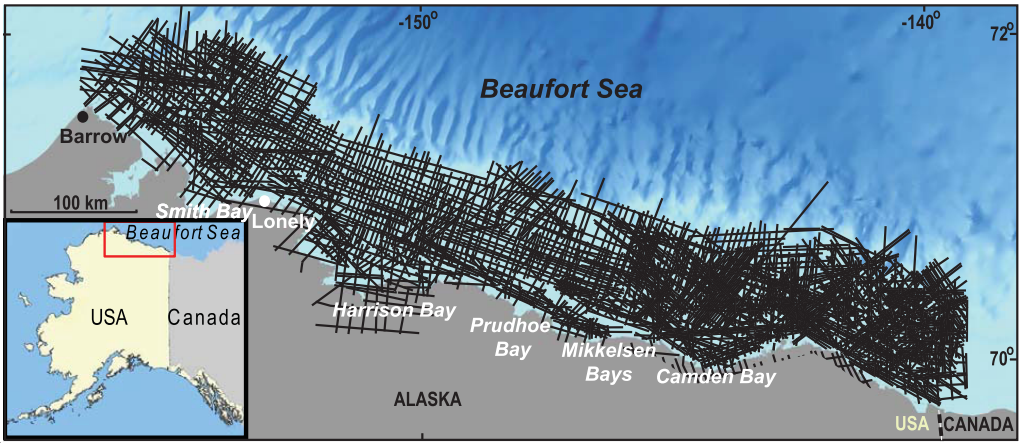

Figure 1. U.S. Beaufort Sea continental shelf and Alaskan North Slope overlain by tracklines (black) of multichannel seismic data used in the velocity analysis (Figure 2 and supporting information). Inset map shows study location (red rectangle).

permafrost may be present, but IBPF may not, include frozen fine-grained sediment that has minimal pore space to hold ice [*Collett and Bird*, 1988], brine-enriched zones within the sediment column [e.g., *Collett and Bird*, 1988, 1993], or thawing rock or sediment with ice-concentration below the resolution of well logs [e.g., *Majorowicz et al*., 2015]. All of these permutations of permafrost likely occur on the U.S. Beaufort shelf to some extent. By definition IBPF is a subset of subsea permafrost.

The U.S. Beaufort continental shelf is 70–120 km wide with an average bathymetric gradient of 1 m/km [*Craig et al*., 1985]. During several Pleistocene sea-level lowstands the shelf was subaerially exposed to the Arctic terrestrial climate conditions [*Dinter*, 1985]. At these times permafrost formed to depths of hundreds of meters, potentially intersecting microbially generated gas formed in situ, or gas that had migrated from a deeper thermogenic source. Either situation would enable the formation of gas hydrate [*Collett et al*., 2011; *Craig et al*., 1985; *Ruppel*, 2015]. During subsequent sea-level high stands, permafrost was exposed to conditions conducive to thawing (i.e., increased temperatures and saline intrusion).

In present times, U.S. onshore IBPF is known to range in thickness from 130 to 650 m [*Collett et al*., 1989; *Osterkamp and Payne*, 1981]. However, IBPF is not vertically continuous, but instead is interrupted by numerous intervals in which the ice content is greatly diminished or absent [*Collett and Bird*, 1993; *Lewis and Collett*, 2013]. Most of the IBPF sequence occurs within a series of flat-lying, laterally-continuous, interbedded Tertiary age sand and shale units [*Craig et al*., 1985]. In the central part of the Alaskan North Slope and the U.S. Beaufort continental shelf, the strata in the upper 650 m of the sediment column consists mainly of the sand-rich Sagavanirktok Formation. In the western portion of the Beaufort the older, prodelta shale facies of Torok Formation and the fluvial-deltaic facies of the Nanushuk Group are present in the upper sediment column [*Bird*, 1988a; *Craig et al*., 1985]. Ranging from 0 to 100 m thickness, the overlying Pleistocene section is a laterally-discontinuous lithologic sequence consisting of massive siltstones to coarse-bedded gravels [*Craig et al*., 1985; *Harding-Lawson*, 1979].

Researchers have used a variety of data sources to map the presence of subsea permafrost (supporting information). Laboratory and field studies indicate that the P-wave velocity of ice-bearing coarse-grained sediments strongly depends on the saturation of ice in pore space. Ice-bonded coarse-grained sediments have velocities from ~2300 to 5000 m s^{-1} [*Rogers and Morack*, 1980; *Timur*, 1968; *Zimmerman and King*, 1986]. On the U.S. and Canadian Beaufort shelf, near-surface unfrozen coarse-grained sediments have velocities of 1700–1900 m s^{-1} [*Hunter et al*., 1978; *Morack and Rogers*, 1984; *Neave and Sellman*, 1982]. Using this velocity contrast between unfrozen and frozen sediments, researchers have interpreted high velocity refractions, identified in MCS data, as subsea IBPF [*Brothers et al*., 2012; *Hunter and Hobson*, 1974; *Hunter et al*., 1978; *MacAulay and Hunter*, 1983; *Neave and Sellman*, 1984; *Pullan et al*., 1987]. *Brothers et al*. [2012] found velocity values ranging from 1700 to 4600 m s^{-1} along the U.S. Beaufort continental shelf. They interpreted refractions in the upper 400 m of the sedimentary column with velocities $\geq$ 2300 m s^{-1} as strata hosting

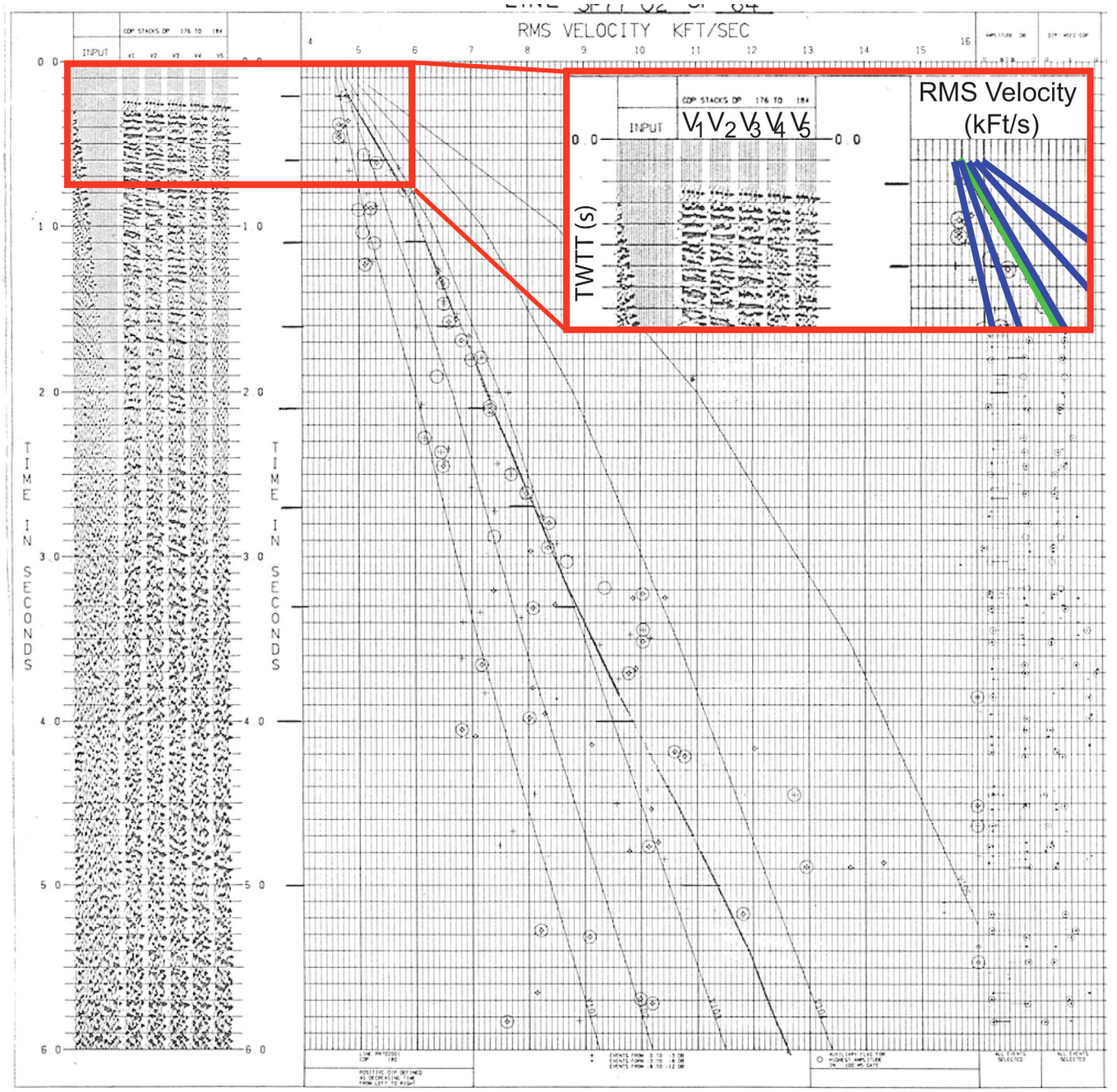

Figure 2. A scanned image of an example of the >50,0000 velocity analyses used in this study. Inset (red box) shows the upper 750 ms TWTT portion of the record that was analyzed. The first plot in the left hand column is the single un-moved out Common Depth Point (CDP) gather at the location of this velocity analysis. The adjacent plots, labeled V1-V5, are stacks of the five adjacent CDPs, each moved out at a different velocity function. The five blue lines on the right-hand plot represent these five velocity functions. The circles are points of high semblance, but due to noise and the occurrence of multiples do not always represent the correct velocity for stacking. The analyst picks the final stacking velocity represented by the green line, using the semblance picks (circles) and the plots of stacked CDPs on the left. In addition to the graph format shown, stacking velocities for a given permit (or survey) were compiled into tables. The upper 750 ms TWTT, excluding the water column, was treated in our analysis, using the Dix equation, as a single interval. Over this interval, where 750 ms TWTT is the base and seafloor is the top, the average velocity was calculated from the stacking velocities.

IBPF. Based on the quarter wavelength criteria, their study, and most refraction studies conducted in the Beaufort, resolved IBPF in thicknesses of 30 m or greater [*Sherwood*, 1967]. *Kang et al.* [2015] used full waveform inversion along four multichannel seismic profiles crossing the Canadian Beaufort shelf to delineate zones of P-wave velocity as high 3500 m s^{-1} that they attributed to subsea IBPF. Other studies have used

seismic velocities in conjunction with well logs or geothermal modeling to map permafrost distribution [*Collett*, 1993; *Frederick and Buffett*, 2015; *Herman*, 2011; *Hu et al*., 2013; *Taylor et al*., 2013].

Numerous studies of circum-arctic subsea permafrost have been conducted at local or regional scales [e.g., *Nicolsky et al*., 2012; *Overduin et al*., 2015; *Rekant et al*., 2005; *Rogers and Morack*, 1980] that cannot fully characterize shelf-wide permafrost distribution. Thus the 100 m isobath, or roughly the shelf edge, remains the defacto seaward extent of continuous permafrost in the arctic [*Brown et al*., 1997]. That delineation is based upon eustatic sea-level rise and limited offshore boreholes [*Bard and Fairbanks*, 1990; *Heginbottom et al*., 1993]. Recent studies on the U.S. Beaufort and South Kara Sea shelves indicate an absence of continuous IBPF seaward of the 20 m isobaths [*Brothers et al*., 2012; *Portnov et al*., 2013]. Examining ~5000 line-km of MCS data, *Brothers et al*. [2012] found no permafrost layer refractions more than 30 km seaward of the modern coastline.

3. Data Sources and Methods

MCS reflection data have been collected for oil exploration on the Federal Outer Continental Shelf of the Beaufort Sea since the mid-1970s under permit to the U.S. Department of Interior. These data are submitted to the Federal government as a condition of the permit and are held proprietary by regulation, generally for 25 years. We examined the stacking velocity (Vstk) data (Figure 2) from 100,000 km of 2D MCS data collected in the Beaufort Sea, as well as from MCS data from onshore portions of the National Petroleum Reserve-Alaska and the Arctic National Wildlife Reserve collected between 1977 and 1990 (Figure 1 and supporting information).

Data examined in this study were collected by different companies, employing various processing techniques (normal moveout, dip corrected moveout, prestack time migration) and using distinct approaches even when applying the same techniques. Of the 50,000 Vstk profiles used (Figure 2), ~20% were reviewed or picked by *Herman* [2011]. Other Vstk profiles were accepted as provided by the companies, except when individual Vstk profiles appeared anomalous compared to adjacent profiles. These anomalous data were discarded if velocity spectra were not available.

We converted the stacking velocity to an average compressional velocity (Vave) using the Dix equation [*Dix*, 1955] at the discrete picked times for each stacking velocity analysis. A cubic spline was then fitted to the Vave at each velocity analysis location, from which Vave was interpolated to 750 ms TWTT. The single interval of 750 ms TWTT nominally corresponds to the uppermost ~600 m of section offshore and possibly >1000 m onshore in permafrost areas, placing it near or below the maximum expected depth of IBPF [*Collett et al*., 1989]. Vave were gridded with 2 km node spacing in GeoFrame where they were smoothed with a two-pass biharmonic filter. Because variation in water depth across the shelf introduces a slight gradient in Vave, using the Dix Equation the velocity of the sediment alone, Vsed, was calculated from:

$$Vsed^2 = \frac{\left(Vave^2 \times 750\ ms\right) - \left(Vwc^2 \times Twc\right)}{750\ ms - Twc}, \tag{1}$$

where *Vsed*= sediment column velocity, *Vave*= velocity from 0 to 750 ms TWTT, *Vwc*= water column velocity 1475 m s^{-1}, and *Twc*=Water column interval TWTT.

In this way the upper 750 ms, excluding the water column is a single interval over which velocity is averaged. Vsed was contoured and its slope derived in ESRI ArcGIS.

4. Velocity Observations

Average sediment column velocities (Vsed) range from 1475 to 3110 m s^{-1}, with higher velocities coinciding with the nearshore areas (Figure 3). The character and gradient of contours change offshore and alongshore. Velocity contours ≥2000 m s^{-1} are tightly spaced (1–8 km apart) and sub parallel with the modern coastline along most of the U.S. Beaufort. Seaward of the 2000 m s^{-1} contour this pattern abruptly changes (Figure 3). Velocity contours <2000 m s^{-1} are spaced more widely apart (up to 90 km). In the mid and outer-shelf, the contours are crenulated and can be punctuated by zones of relatively higher bulk velocities. The first derivative, or slope, of the mapped velocities, highlights where velocity changes the most rapidly in the study area (Figure 4). Velocity changes the most rapidly

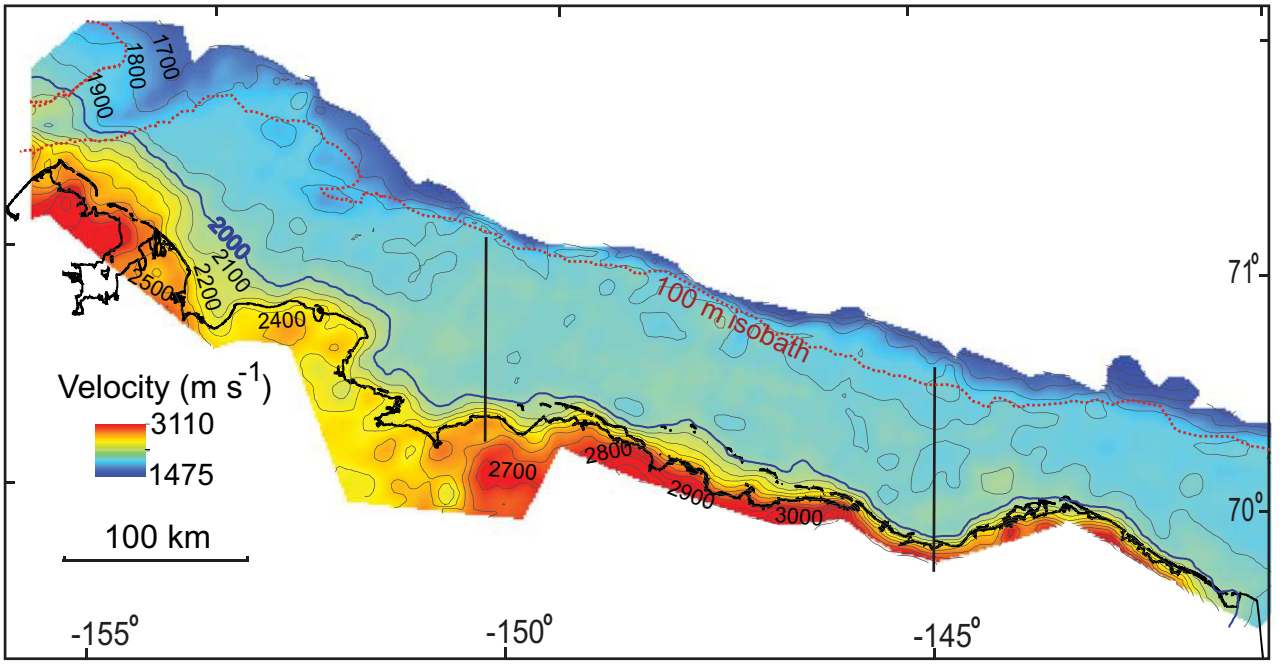

Figure 3. Gridded Dix average velocities (Vsed) for the upper 750 ms TWTT. For marine data, the interval velocity was calculated from the seafloor down to 750 ms of the total TWTT (equation (1)). Contour lines are every 100 m s^{-1}. Velocities vary monotonically with the maximum values occurring onshore while the lowest values occur offshore. The 2000 m s^{-1} contour is blue. Shore perpendicular black lines indicate locations of profiles shown in Figure 5. The location of the 100 m isobath is shown as a red, dotted line.

along the modern shoreline, at the shelf edge and along Barrow Canyon (Figure 3). Rapid changes in velocity along the shelf edge and Barrow Canyon likely reflect the diminution of sediment in the upper 750 ms TWTT as the water depth plunges in those areas. The shelf's velocity pattern flattens abruptly at the 2000 m s^{-1} contour over the entire U.S. Beaufort continental shelf (Figures 3–5).

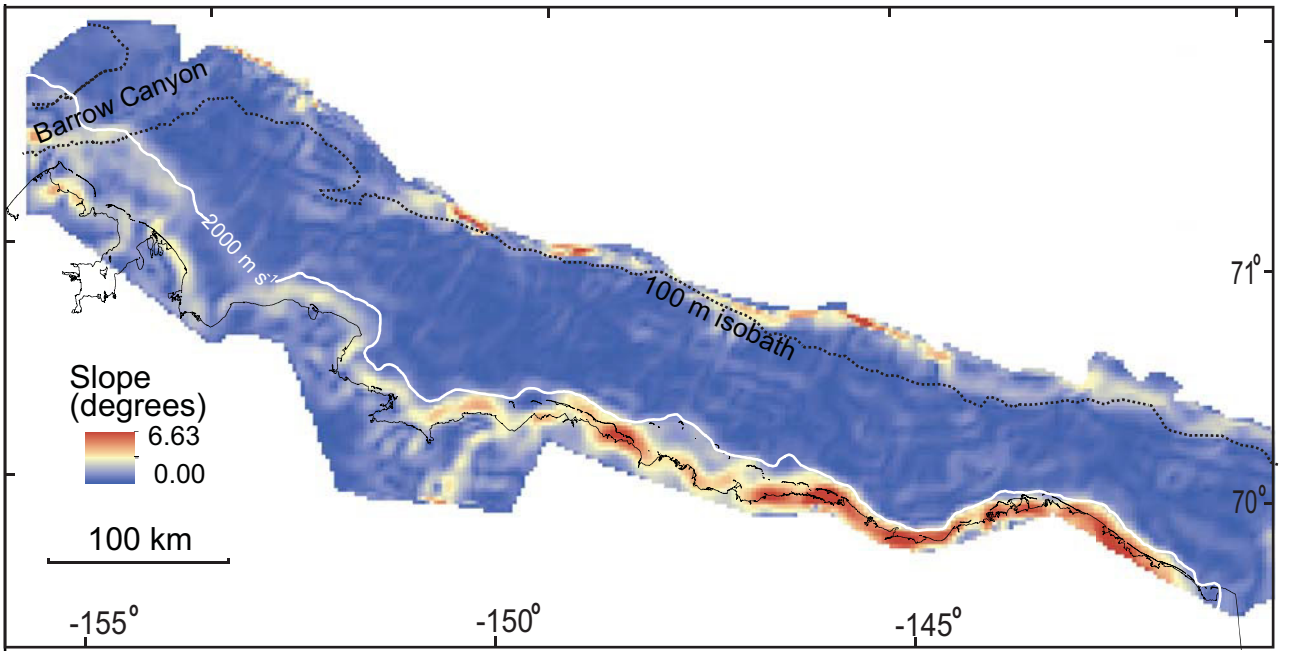

Figure 4. Slope of U.S. Beaufort continental shelf velocity structure. The zones of most rapid change in the interval velocities loosely parallel the Alaskan coastline. Elevated values are also observed near the shelf edge where the sediment portion of the upper 750 ms TWTT rapidly diminishes. For reference the locations of the 2000 m s^{-1} contour (white line) and 100 m isobath (black, dotted line) are also shown.

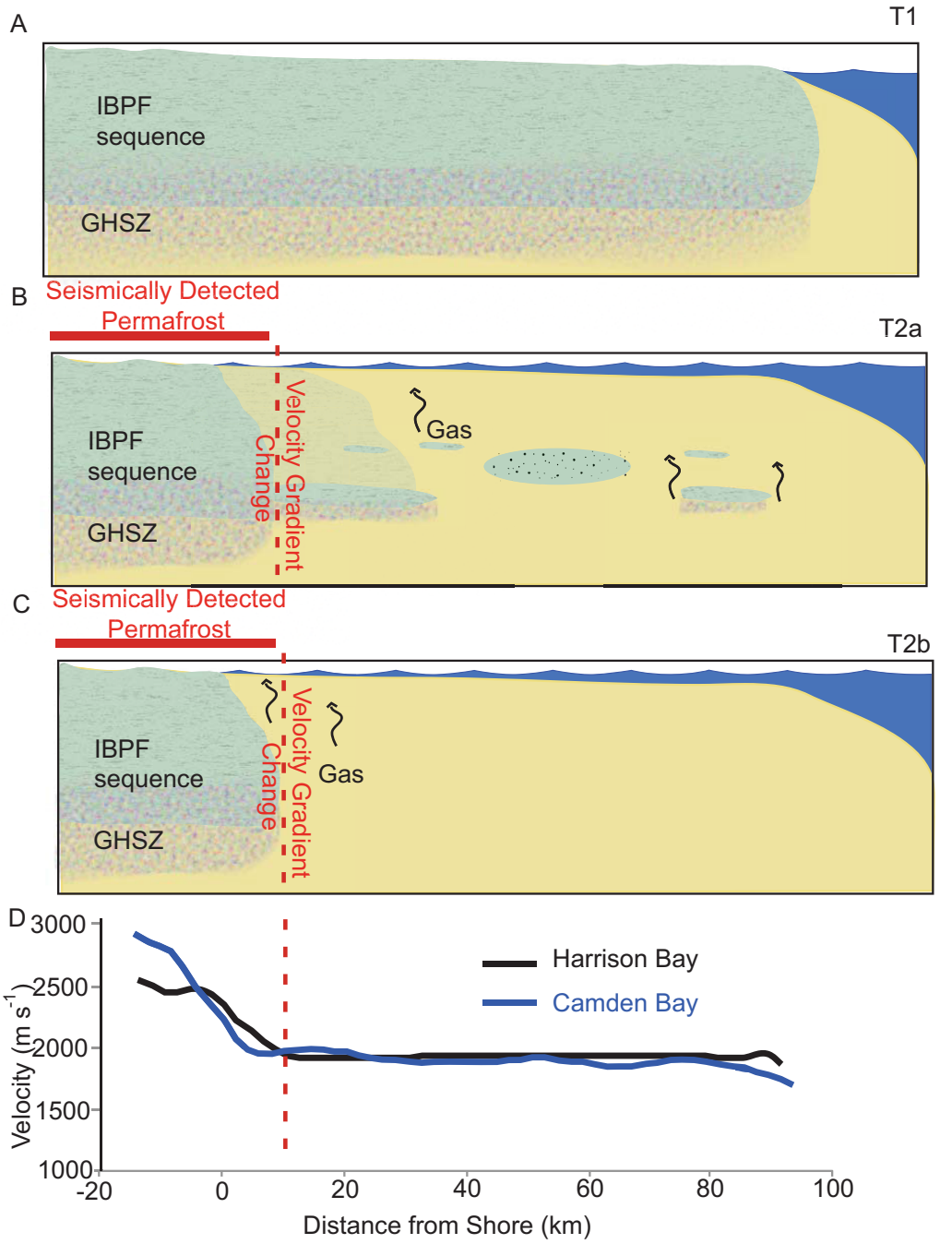

Figure 5. (a) A schematic cross section of the U.S. Beaufort continental shelf at sea level low stand in the Late Pleistocene. The IBPF sequence and gas hydrate stability zone (GHSZ) extend to the shelf edge. (b) The present-day continental shelf. Seismic observations suggest that a continuous wedge of IBPF exists onshore and degrades rapidly seaward of the modern shoreline with minimal permafrost >37 km from the modern shoreline. Subsea permafrost may occur in the mid and outer shelf in quantities or conditions that are below the resolution of our methods. (c) Present-day conditions with the minimum IBPF distribution inferred from the seismic reflection velocity analyses method. (d) The onshore-offshore velocity profiles from Harrison Bay (black) and Camden Bay (blue) show an abrupt decrease in slope within 20 km of shore. Dashed red line emphasizes the break in velocity gradient. See Figure 3 for profile locations.

5. Discussion

5.1. U.S. Beaufort Shelf Velocity and Subsea IBPF Distribution

The vertical distribution of IBPF within the sediment column is not captured with the seismic reflection velocity analyses method employed here. The individual interbedded zones of IBPF (high velocity) and

unfrozen/low ice-content material (low velocity) that are known from well logs to typify the IBPF sequence in the onshore and nearshore environment [e.g., *Collett and Bird*, 1993; *Harding-Lawson*, 1979; *Lewis and Collett*, 2013] are not resolved with this technique because velocities are averaged from the seabed to 750 ms TWTT. The Vsed value in two locations could be the same, but the character of the IBPF sequence (number or thickness of interbedded IBPF layers, ice content, grain size, etc.) could differ. Instead, the seismic reflection velocity analyses method indicates the net effect of high velocity IBPF in the upper sediment column. When examined in plan view, it is clear that the net effect of IBPF is far greater onshore than it is offshore (Figure 3).

Despite differences in methods and sources used to acquire and process the stacking velocities used in this study, Vsed values vary monotonically across the U.S. Beaufort shelf with the highest velocities occurring entirely onshore while minimum velocity values occur exclusively offshore (Figure 3). Highest velocities ($>$3000 m s^{-1}) coincide with the thickest occurrences of onshore IBPF [*Collett et al*., 1989]. Velocity contours are most tightly spaced near the present-day shoreline (Figure 3) and then the rate of change in velocity dramatically decreases across the inner shelf (Figures 4 and 5). Though margin-wide geology is not uniform [e.g., *Bird*, 1988b] and changes in lithology can impact interval velocities, no lithological features within the permafrost zone strata (upper 750 ms TWTT) have been reported [*Craig et al*., 1985; *Grantz and May*, 1984] that would explain margin-wide abrupt shore-parallel decreases in velocity. Thus, we interpret the distribution of seismic velocities as further evidence for an abundance of IBPF onshore and minimal, if any, IBPF through the shelf edge. Further, we interpret the tightly-spaced, shore-parallel velocity contours as the seaward termination of the continuous subsea IBPF sequence (Figure 5) and use the 2000 m s^{-1} contour as a proxy for this transition.

The 2000 m s^{-1} contour generally occurs within 20 km of shore, and landward of the 25 m isobath. The greatest change in velocity over the shortest distance, occurs in the eastern third of the margin where the 2000 m s^{-1} contour nearly coincides with the modern shoreline (Figure 4). We interpret the rapid diminution in velocity as an indication that continuous IBPF degrades seaward most rapidly in this area. This rapid seaward degradation of IBPF may potentially relate to the eastern portion of the study area having an earlier inundation history, as inferred from bathymetry [*Amante and Eakins*, 2009], and/or possibly relate to faulting and potential vertical fluid migration beneath Camden Bay and the area north of the Brooks Range mountains [*Craig et al*., 1985; *Grantz and May*, 1982]. Of those two mechanisms, the existence of a thick IBPF sequence onshore [*Collett et al*., 1989] suggests that inundation plays a more important role in IBPF degradation than any potential vertical water movement through faults. In the northwestern portion of the study area the 2000 m s^{-1} contour is 37 km from Smith Bay's modern shoreline (Figure 3). The elevated, offshore velocities may reflect the shallowness of older, underlying geologic units in that area (i.e., the Nanushuk Group, the Torok Formation) [*Bird*, 1988a; *Grantz and May*, 1984]. *Osterkamp and Payne* [1981] also noticed a correspondence between permafrost and rock type near Prudhoe and Mikkelson Bays, central North Slope.

Although our study cannot resolve the character of the IBPF sequence within the sediment column, we can estimate the proportion of the IBPF in the sedimentary column necessary to produce an average velocity of 2000 m s^{-1} using an arithmetic mixing relationship in the form:

$$2000\ \text{m s}^{-1} = x \cdot v_{IBPF} + [1-x] \cdot 1875\ \text{m s}^{-1}, \quad (2)$$

where: 2000 m s^{-1} is the velocity associated with the seaward termination of continuous IBPF, x is the fraction of the sedimentary column that contains IBPF, V_{IBPF} is the velocity of IBPF, and 1875 m s^{-1} is used as the background non-IBPF sediment velocity. *Brothers et al.* [2012] identified IBPF refraction layers with velocities ranging from 2300 m s^{-1} to 4500 m s^{-1}. A sedimentary column that contains high-velocity IBPF (V_{IBPF} = 4500 m s^{-1}) need only consist of ~5% IBPF, while a sedimentary column that has layers with low-velocity IBPF (V_{IBPF} = 2300 m s^{-1}) will need 29% of the column to contain IBPF to have a Vsed = 2000 m s^{-1}. This demonstrates the possible range of IBPF concentrations at Vsed = 2000 m s^{-1}. IBPF may exist seaward of the 2000 m s^{-1} contour, but makes up a low proportion of the sediment column. *Ruppel et al.* [2016] characterize the nuances of vertical IBPF distribution and examines IBPF concentration in their analysis of offshore borehole logs.

We note that increasing water depth can impact average velocities (Vave) of the upper 750 ms TWTT. Removing the water column from the average velocities (equation (1)) causes the thickness of sediments

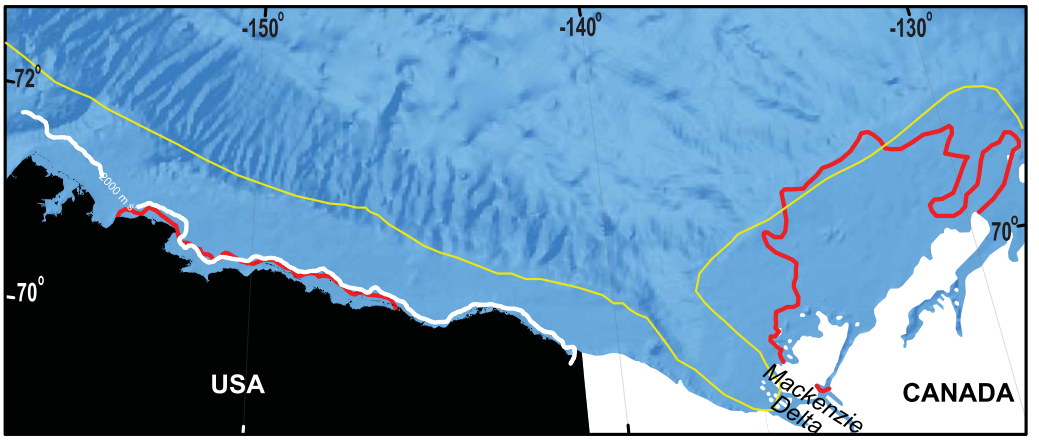

Figure 6. Map of subsea IBPF indicators on the U.S. & Canadian Beaufort. The yellow line is the proposed near-shelf edge boundary [*Brown et al.*, 1997]. Red lines indicate the seaward extent of subsea permafrost determined by seismic refraction analysis [*Brothers et al.*, 2012; *Hunter et al.*, 1978; *Pullan et al.*, 1987]. White line is the 2000 m s^{-1} contour.

represented by Vsed to thin seaward. For example, the sediment column used for average sediment velocity (Vsed) at the 100 m bathymetric contour is ~100 m thinner than the sediment column used in the average sediment velocity (Vsed) at the shoreline. Sediments or rock deeper down in the subbottom tend to have higher velocities than more shallow sediments due to the consolidation of sediment and compaction of pore space [e.g., *Hamilton*, 1979]. Thus, eliminating the contribution of the deepest 100 m of sediment would have the effect of lowering Vsed at deeper water depths, independent of the changing IBPF content. However, across the very flat and slowly dipping U.S. Beaufort continental shelf [*Craig et al.*, 1985], this effect on the velocity (Vsed) is small (<2%) (see supporting information for calculation) and the nearshore peak change in Vsed that we interpret as changes in continuous IBPF distribution does not correspond to the peak change in water depth (Figures 3 and 4). In addition, downhole log data indicate that the upper 800 m of strata are composed of unconsolidated silts, sands and gravels instead of highly compacted bedrock [*Ruppel et al.*, 2016].

Seaward of the shelf break, near the 100 m isobath, water depth increases rapidly and the effect on Vsed (defined as the average velocity from the seafloor to 750 ms TWTT) is pronounced (Figure 3 and 4). Water depths reach 553 m (e.g., 750 ms TWTT in water) within 5 km of the 100 m isobath in the western Beaufort Sea and within 25 km of the 100 m isobath in the eastern Beaufort Sea [*Amante and Eakins*, 2009]. No sediment column at all would be included in a calculation of Vsed seaward of the 553 m isobaths. For this reason, our analysis is restricted to the area of the physiographic shelf, where water depths are less than 100 m. We also note that no permafrost is expected beyond the shelf break because the seafloor there was never subaerially exposed [e.g., *Brigham and Miller*, 1984; *Collett and Dallimore*, 2003].

5.2. Other Constraints on U.S. Beaufort Subsea Permafrost Distribution

In their study, *Brothers et al.* [2012] mapped seismic refractions found in the upper 400 m of the sedimentary column that had velocities ≥ 2300 m s^{-1}. They interpreted these refractions as discrete strata tens of meters thick [*Sherwood*, 1967] containing IBPF. Whereas the refraction method can identify IBPF that occurs in discrete layers, the seismic reflection velocity analyses method characterizes the net effect IBPF-associated velocities have on the sediment column. In general, the seaward extent of continuous IBPF determined from high velocity (≥ 2300 m s^{-1}) refractions corresponds with the 2000 m s^{-1} contour along the U.S. Beaufort (Figure 6).

Nonseismic studies of U.S Beaufort continental shelf IBPF also suggest that the shelf edge may be an over estimation of present-day continuous IBPF distribution. Two-dimensional finite element studies of *Osterkamp and Fei* [1993] and *Romanovsky and Osterkamp* [1996] found continuous IBPF to terminate within 8–50 km of the modern shoreline at Barrow and Lonely, Alaska. *Collett et al.* [1988] put the seaward extent of continuous IBPF near the 50 m (or less) water depth contour based on well logs and geothermal modeling. Although nearshore wells confirm the presence of IBPF landward of the 2000 m s^{-1} contour [*Collett and Bird*, 1993; *Collett et al.*, 1988; *Harding-Lawson*, 1979; *Lewis and Collett*, 2013; *Ruppel et al.*, 2016], borehole

evidence for the widespread presence of subsea IBPF nearshore and across the shelf is variable [*Amoco*, 1988; *Harding-Lawson*, 1979; *Ruppel et al*., 2016].

There are many conditions that could contribute to heterogeneous distribution of subsea IBPF or permafrost in the continental shelf. Our method delivers a regional-scale interpretation of continuous subsea IBPF distribution and indicates that IBPF becomes significantly less abundant in the sediment column seaward of the 2000 m s^{-1} contour. However, it is possible that local heterogeneities below the 2 km resolution of our gridded velocities, such as paleochannels [e.g., *Northern Land Use Research*, *Inc*., 2007], cryopegs [*Collett and Bird*, 1993], and lithologic variation [*Osterkamp and Payne*, 1981], cause the IBPF sequence to be absent in some portions of the U.S. Beaufort continental shelf landward of the 2000 m s^{-1} contour.

It is also possible that subsea IBPF and permafrost exist seaward of the 2000 m s^{-1} contour. If subsea IBPF exists seaward of the 2000 m s^{-1} contour, it occurs in discontinuous lenses below the resolution of either seismic refraction or seismic reflection velocity methods (Figure 5b). Fine-grained lithology [*Collett and Bird*, 1988; *Morack and Rogers*, 1984], widespread saline intrusion [*Osterkamp et al*., 1989], minimal ice-content due to thawing [*Majorowicz et al*., 2015] or possibly preinundation lake and drainage patterns [e.g., *Romanovskii* et al., 2000] are all scenarios that could contribute to occurrences of subsea permafrost seaward of the 2000 m s^{-1} contour. We stress that although those conditions of subsea permafrost may exist in the U.S. Beaufort continental shelf, our method cannot detect them. In this way our seaward boundary set by the 2000 m s^{-1} contour, is a minimum seaward extent of instances of subsea permafrost (Figure 5c).

The model of continuous IBPF rapidly thinning seaward of the modern shoreline with subsequent thin and discontinuous occurrences is also suggested by recent studies in the South Kara Sea [*Portnov et al*., 2014, 2013]. In addition to using high-resolution seismic data, *Portnov et al*. [2013] collected water column data. They identified hydroacoustic anomalies characteristic of seafloor gas emissions [*Greinert et al*., 2010] along interpreted boundaries of subsea permafrost. Their studies, along with work conducted in the East Siberian and Canadian Beaufort shelves relate seafloor methane emissions to subsea permafrost degradation [*Paull et al*., 2011; *Serov et al*., 2015; *Shakhova et al*., 2010]. *Portnov et al*. [2013] suggest that continuous subsea permafrost acts as a seal for gas sourced below the permafrost (e.g., from gas hydrate or deeper thermogenic sources) and with degradation gas migrates up along the seaward edge of continuous subsea permafrost. Both the Canadian Beaufort and the West Kara shelves host pingo-like features associated with seabed fluid escape [*Paull et al*., 2007; *Portnov et al*., 2013; *Serov et al*., 2015]. Though neither pingo-like features nor seafloor degassing have ever been observed on the U.S. Beaufort, we suggest that the vicinity of the 2000 m s^{-1} contour is the locus at which degassing related to IBPF degradation is most likely to occur.

5.3. Differences Between the Canadian and U.S. Beaufort Shelves

Subsea permafrost distribution varies markedly on the U.S. and Canadian Beaufort margins (Figure 6). The offshore extent of continuous IBPF on the U.S. portion of the Beaufort margin is limited to within 37 km of the modern shoreline (generally less than 20 m water depth). In contrast, using the same or very similar methods, continuous subsea IBPF has been inferred to ~150 km offshore the present-day Canadian shoreline occupying nearly the entire shelf. For example, whereas *Kang et al*.'s [2015] full wave form inversion study mapped velocity values of 3000–3500 m s^{-1} in the outer shelf, *Brothers et al*. [2012] and this study only identified those same IBPF-related elevated velocities onshore or in the nearshore (Figures 3 and 6).

Several differences in geologic setting and climate history may account for variation in subsea permafrost patterns along the Beaufort margin. To begin with, the western part of the Beaufort Shelf is a classic passive margin, while the region of Camden Bay and east is in a compressional regime produced as the Brooks Range pushes north into the Beaufort Sea [*Craig et al*., 1985; *Grantz and May*, 1982]. Faulting could contribute to upward migration of warm fluids causing a distinct regional heat flux pattern. Glaciation likely also plays a role in IBPF distribution. We note that continuous IBPF does not uniformly extend to the Canadian shelf edge (Figure 6) [*Hu et al*., 2013]. There is a lack of permafrost, for the most part, beneath the active channel of the Mackenzie River (Figure 6). The significant westward decrease in IBPF on the Canadian Beaufort may relate to a middle-to-late Wisconsin ice advance of a wet-based glacier that overrode the present Mackenzie River channel [*Beget*, 1987]. The warm glacier may have inhibited IBPF through elevated temperatures and/or loading that may have deformed the underlying sand and clay units and destroyed their internal stratigraphy, making those sediments less conducive to maintaining ice in the pore space [*Blasco et al*., 1987].

Because inundation is a key factor in permafrost degradation, differences in relative sea-level histories related to proximity to the Laurentide ice sheet or shelf slope might also explain the contrasting subsea permafrost regimes on the U.S. and Canadian sides of the Beaufort Sea margin [*Amante and Eakins*, 2009; *Dyke et al*., 2002; *Hill et al*., 1993; *Hill et al*., 1985; *Northern Land Use Research, Inc*., 2007]. Differences between the distributions of subsea permafrost on the U.S. and Canadian margins could also be the result of the permafrost having evolved to different states before the instigation of sea-level rise, possibly due to being subjected to different conditions since the end of the LGM (e.g., ice sheet dynamics), differences in offshore lithologies, groundwater discharge [*Frederick and Buffett*, 2015] or a combination of these factors.

Lastly, the Canadian Beaufort margin is dominated by the Mackenzie River Delta with a sediment load and coastal presence very distinct from anything present in the U.S. Beaufort [*Blasco et al*., 2013; *Hopkins and Hartz*, 1978]. The Mackenzie Delta is dominated by fresh-water flow and fresh-water bedflow, whereas the U.S. Beaufort seabed could be more brine rich. Widespread salt intrusion into pore space, which thaws ice and lowers the freezing temperature [*Osterkamp et al*., 1989], is one possible mechanism responsible for the IBPF degradation that we infer on the U.S. Beaufort margin, and this process is likely less active on the Canadian Beaufort margin. We offer these hypotheses for discussion, recognizing the reasons for differences between the two shelves will remain speculative until a systematic pan-Beaufort study of subsea IBPF distribution is conducted.

6. Conclusions

Using the stacking velocities from 100,000 km of industry seismic data, we infer that the continuous IBPF sequence exists close to shore along the entire extent of the U.S. Beaufort margin and thins rapidly seaward. The interpreted seaward edge of this continuous IBPF, the 2000 m s^{-1} contour, is everywhere at contemporary water depths of less than 25 m, and within 37 km of the modern shoreline. Our method produces a shelf-scale map of minimum areal distribution of ice-bearing permafrost. Seaward of the continuous IBPF, permafrost or relict IBPF may exist in small quantities. Our results show that U.S. Beaufort subsea permafrost has degraded substantially since Pleistocene lowstand and, when taken into account with other regional observations, the shelf-edge should be dismissed as the presumed extent of continuous IBPF.

Acknowledgments
BOEM and DOE-USGS Interagency Agreement DE-FE0002911 supported this research. L.B. was supported by a DOE NETL/NRC Methane Hydrate Fellowship under DE-FC26-05NT42248. C.R. was supported by USGS–DOE Interagency Agreements DE-FE000291 and 0023495. We thank Tim Collett, Bill Schwab, Krissy Lewis, Matt Frye for support, data files and critical discussions. Tim Collett, David Foster, Susan Banet, Warren Wood and an anonymous reviewer provided helpful reviews. Any use of trade, firm, or product names is for descriptive purposes and does not imply endorsement by the U.S. Government. A subset of the data used in this study is available from the National Archive of Marine Seismic Surveys https://walrus.wr.usgs.gov/NAMSS/. All data used in this study may be requested from the Bureau of Ocean Energy Management (BOEM) (see supporting information).

References

Amante, C., and B. W. Eakins (2009), ETOPO1 1 arc-minute global relief model: Procedures, data sources and analysis, *NOAA Tech. Memo. NESDIS NGDC-24*, Natl. Geophys. Data Cent., NOAA, Boulder, Colo., doi:10.7289/V5C8276M.

Amoco (1988), Final Well Report Amoco Production Company Amoco Belcher OCS-Y-0917-1 Beaufort Sea, Offshore Alaska, USA September 1988 through October 1988, edited by M. M. Service, Miner. Manage. Serv., Anchorage, Alaska.

Bard, H. B., and R. G. Fairbanks (1990), U-Th ages obtained by mass spectrometry in corals from Barbados: Sea level during the past 130,000 years, *Nature*, *346*, 456–458, doi:10.1038/346456a0.

Beget, J. (1987), Was the Late Pleistocene northwest Laurentide Ice Sheet wet-based?, in *Late Cenozoic History of the Interior Basins of Alaska and the Yukon, U.S. Geol. Surv. Circ. 1026*, edited by D. Carter, T. D. Hamilton and J. P. Galloway, pp. 22–24, Dep. of the Inter., Washington, D. C.

Bird, K. J. (1988a), Alaskan North Slope stratigraphic nomenclature and data summary for government-drilled wells, in *Geology and Exploration of the National Petroleum Reserve in Alaska, 1974 to 198, U.S. Geol. Surv. Prof. Pap. 1399*, edited by G. Gryc, pp. 317–353, U.S. Gov. Print. Off., Washington D. C.

Bird, K. J. (1988b), Structure-contour and isopach maps of the national petroleum reserve in Alaska, in *Geology and Exploration of the National Petroleum Reserve in Alaska, 1974 to 198, U.S. Geol. Surv. Prof. Pap. 1399*, edited by G. Gryc, pp. 355–377, U.S. Gov. Print. Off., Washington, D. C.

Blasco, S., et al. (2013), 2010 State of Knowledge: Beaufort Sea seabed geohazards associated with offshore hydrocarbon development, *Geol. Surv. of Can., Open File Rep*. 6989, 340 pp.

Blasco, S. M., J. K. Brigham-Grette, and P. R. Hill (1987), Offshore constraints on the Late Pleistocene glacial history at the mouth of the Mackenzie River, in *Late Cenozoic History of the Interior Basins of Alaska and the Yukon, U.S. Geol. Surv. Circ. 1026*, edited by D. Carter, T. D. Hamilton and J. P. Galloway, pp. 15–17, Dep. of the Inter., Washington, D. C.

Brigham, J. K., and G. H. Miller (1984), Paleotemperature estimates of the Alaskan Arctic Coastal Plain during the last 125,000 years, in *Proceedings of the Fourth International Conference on Permafrost*, pp. 80–85, Natl. Acad. Press, Washington, D. C.

Brothers, L. L., P. E. Hart, and C. D. Ruppel (2012), Minimum distribution of subsea ice-bearing permafrost on the US Beaufort Sea continental shelf, *Geophys. Res. Lett.*, *39*, L15501, doi:10.1029/2012GL052222.

Brown, J., J. Ferrians, O.J., J. A. Heginbottom, and E. S. Menikov (1997), *Circum-Arctic Map of Permafrost and Ground-Ice Conditions*, U.S. Geol. Surv. in cooperation with the Circum-Pac. Counc. for Energy and Miner. Resour., Washington, D. C.

Collett, T. S. (1993), Natural gas hydrates of the Prudhoe Bay and Kuparuk River Area, North Slope, Alaska, *AAPG Bull.*, *77*(5), 793–812.

Collett, T. S., and K. J. Bird (1988), Freezing-point depression at the base of ice-bearing permafrost of the North Slope of Alaska, in *5th International Conference on Permafrost*, pp. 50-57, Tapir Publ., Trondheim, Norway.

Collett, T. S., and K. J. Bird (1993), Unfrozen, high-salinity intervals within ice-bearing Permafrost, North Slope of Alaska, in *6th International Conference on Permafrost*, pp. 1-7, South China Univ. of Technol. Press, Beijing.

Collett, T. S., and S. R. Dallimore (2003), Permafrost-associated gas hydrate, in *Natural Gas Hydrate in Oceanic and Permafrost Environment*, edited by M. D. Max, pp. 43–60, Kluwer Acad., Dordrecht, Netherlands.
Collett, T. S., K. J. Bird, K. A. Kvenvolden, and L. B. Magoon (1988), Geologic interrelations relative to gas hydrates within the North Slope of Alaska, *U.S. Geol. Surv. Open-File Rep., 88-389*, 150 pp.
Collett, T. S., K. J. Bird, K. A. Kvenvolden, and L. B. Magoon (1989), Map Showing the Depth to the Base of the Deepest Ice-Bearing Permafrost as Determined From Well Logs, North Slope, Alaska, *U.S. Geol. Surv. Oil Gas Invest. Map*, 222 pp.
Collett, T. S., M. W. Lee, W. F. Agena, J. J. Miller, K. A. Lewis, M. V. Zyrianova, R. Boswell, and T. L. Inks (2011), Permafrost-associated natural gas hydrate occurrences on the Alaska North Slope, *Mar. Pet. Geol.*, *28*(2), 279–294.
Craig, J. D., K. W. Sherwood, and P. P. Johnson (1985), Geologic report for the Beaufort Sea Planning Area, Alaska: Regional Geology, Petroleum Geology, Environmental Geology, *OCS Rep. MMS 85-0111*, 192 pp., Alaska OCS Region.
Dinter, D. A. (1985), Quaternary sedimentation of the Alaskan Beaufort shelf- influence of regional tectonics, fluctuating sea levels and glacial sediment sources, *Tectonophysics*, *114*, 133–161.
Dix, C. (1955), Seismic velocities from surface measurements, *Geophysics 20*(1), 68–86.
Dyke, A. S., J. T. Andrews, P. U. Clark, J. H. England, G. H. Miler, J. Shaw, and J. J. Veillette (2002), The Laurentide and Innuitian ice sheets during the Last Glacial Maximum, *Quat. Sci. Rev.*, *21*, 9–31.
Frederick, J. M., and B. A. Buffett (2015), Effects of submarine groundwater discharge on the present-day extent of relict submarine permafrost and gas hydrate stability on the Beaufort Sea continental shelf, *J. Geophys. Res. Solid Earth*, *120*, 417–423, doi:10.1002/2014JF003349.
Grantz, A., and S. D. May (1982), Rifting history and structural development of the continental margin north of Alaska, in *Studies in Continental Margin Geology*, edited by J. S. Watkins and C. L. Drake, AAPG Mem., 34, pp. 77–102.
Grantz, A., and S. D. May (1984), Summary geologic report for Barrow Arch Outer Continental Shelf (OCS) Planning Area, Chukchi Sea, Alaska, *U.S. Geol. Surv. Open-File Rep. 84-395*, 44 pp.
Greinert, J., D. F. McGinnis, L. Naudts, P. Linke, and M. De Batist (2010), Atmospheric methane flux from bubbling seeps: Spatially extrapolated quantification from a Black Sea shelf area, *J. Geophys. Res.*, *115*, C01002, doi:10.1029/2009JC005381.
Hamilton, E. L. (1979), Sound velocity gradients in marine sediments, *J. Acoust. Soc. Am.*, *65*(4), 909–922.
Harding-Lawson Associates (HL) (1979), USGS Technical Investigation Beaufort Sea-1979, vol. 1–2, 452 pp.
Heginbottom, J. A., J. Brown, E. S. Melnikov, and O. J. Ferrians Jr. (1993), Circum-Arctic map of permafrost and ground ice conditions, in *6th International Conference on Permafrost*, pp. 1132-1136, South China Univ. of Technol. Press, Beijing.
Herman, B. M. (2011), The distribution of permafrost beneath the Beaufort Sea Continental Shelf, Abstract #C31A-0590 presented at 2011 Fall Meeting, AGU, San Francisco, Calif.
Hill, P. R., P. J. Mudie, K. Moran, and S. M. Blasco (1985), A sea-level curve for the Canadian Beaufort Shelf, *Can. J. Earth Sci.*, *22*(10), 1383–1393, doi:10.1139/e85-146.
Hill, P. R., A. Hequette, and M.-H. Ruz (1993), Holocene sea-level history of the Canadian Beaufort shelf, *Can. J. Earth Sci.*, *30*, 103–108.
Hopkins, D. M., and R. W. Hartz (1978), Coastal morphology, coastal erosion, and barrier islands of the Beaufort Sea, Alaska, *U.S. Geol. Surv. Open-File Rep.*, 78–1063, 58 pp.
Hu, K., Z. Issler, Z. Chen, and T. A. Brent (2013), Permafrost investigation by well logs, and seismic velocity and repeated shallow temperature surveys, Beaufort-Mackenzie Basin, *Geol. Surv. Can. Open File Rep., 6956*, 228 pp.
Hunter, J. A., and G. D. Hobson (1974), Seismic refraction method of detecting sub-sea bottom permafrost, in *The Coast and Shelf of the Beaufort Sea*, edited by J. C. Reed and J. E. Sater, pp. 401–415, Arctic Inst. of North Am., San Francisco, Calif.
Hunter, J. A., K. G. Neave, H. A. MacAulay, and G. D. Hobson (1978), Interpretation of sub-seabottom permafrost in the Beaufort Sea, in *Third International Conference on Permafrost*, edited by C. B. Crawford, pp. 514-520, Natl. Res. Counc. of Can., Edmonton, Alberta, Canada.
Kang, S.-G., J. K. Hong, Y. K. Jin, S. Kim, Y.-G. Kim, M. Riedel, S. Dallimore, and C. Shin (2015), P-wave velocity models using full waveform inversion for the permafrost in the Canadian Shelf of Beaufort Sea, Arctic, Abstract B31D-0588 presented at 2015 Fall Meeting, AGU, San Francisco, Calif.
Kvenvolden, K. A., and A. Grantz (1990), Gas hydrates of the Arctic Ocean, in *The Arctic Region. The Geology of North America*, edited by A. Grantz, L. Johnson and J. F. Sweeney, pp. 539–549, Geol. Soc. Am., Boulder, Colo.
Lewis, K. A., and T. S. Collett (2013), Brookian Sequence well log correlation sections and occurrence of gas hydrates, north-central North Slope, Alaska, *U.S. Geol. Surv. Sci. Invest. Rep., 2013-5050*, 33 pp.
MacAulay, H. A., and J. A. Hunter (1983), Detailed seismic refraction analysis of ice-bonded permafrost layering in the Canadian Beaufort Sea, paper presented at 4th Canadian Permafrost Conference, Natl. Res. Counc. of Can., Calgary, Alberta, Canada.
Majorowicz, J., K. Osadetz, and J. Safanda (2015), Models of talik, permafrost and gas hydrate histories–Beaufort Mackenzie Basin, Canada, *Energies*, (*8*), 6738–6764, doi:10.3390/en8076738.
Morack, J. L., and J. C. Rogers (1984), Acoustic velocities of nearshore materials in the Alaskan Beaufort and Chukchi Seas, in *The Alaskan Beaufort Sea: Ecosystems and Environments*, edited by P. W. Barnes, D. M. Schell and E. Reimnitz, pp. 259–274, Academic, Orlando, Fla.
National Snow & Ice Data Center (2016), Cryosphere Glossary. [Available at https://nsidc.org/cryosphere/glossary/, last accessed 28 Sept 2016.]
Neave, K. G., and P. V. Sellman (1982), Subsea permafrost in Harrison Bay, Alaska, An interpretation from seismic data, *CRREL Rep. 82-24*, 62 pp., Hanover, N. H.
Neave, K. G., and P. V. Sellman (1984), Determining distribution patterns of ice-bonded permafrost in the U.S. Beaufort sea from seismic data, in *The Alaskan Beauforrt Sea: Ecosystems and Environments*, edited by P. W. Barnes, D. M. Schell, and E. Reimnitz, pp. 237–258, Academic, Orlando, Fla.
Nicolsky, D. J., V. E. Romanovsky, N. N. Romanovskii, A. L. Kholodov, N. E. Shakhova, and I. P. Semiletov (2012), Modeling sub-sea permafrost in the East Siberian Arctic Shelf: The Laptev Sea region, *J. Geophys. Res.*, *117*, F03028, doi:10.1029/2012JF002358.
Northern Land Use Research, Inc. (2007), Review of geological/geophysical data and core analysis to determine archaeological potential of buried landforms, Beaufort Sea Shelf, Alaska, *OCS Study MMS Rep. 2007-004*, 25 pp., Alaska OCS Region.
Osterkamp, T. E., and T. Fei (1993), Potential occurrence of permafrost and gas hydrates in the continental shelf near Lonely, Alaska, in *6th International Conference on Permafrost*, pp. 500–505, South China Univ. of Technol. Press, Beijing, China.
Osterkamp, T. E., and J. P. Gosink (1991), Variations in permafrost thickness in response to changes in paleoclimate, *J. Geophys. Res.*, *96*(B3), 4423–4434.
Osterkamp, T. E., and M. W. Payne (1981), Estimates of permafrost thickness from well logs in northern Alaska, *Cold Reg. Sci. Technol.*, *5*, 13–27.
Osterkamp, T. E., G. C. Baker, W. D. Harrison, and T. Matava (1989), Characteristics of the active layer and shallow subsea permafrost, *J. Geophys. Res.*, *94*(C11), 16,227–16,236.

Overduin, P. P., S. Wetterich, F. Gunther, M. N. Grigoriev, G. Grosse, L. Schirrmeister, H. W. Hubberten, and A. Makarow (2015), Coastal dynamics and subsea permafrost in shallow water of the central Laptev Sea, East Siberia, *Cryosphere Discuss.*, *9*, 1–35, doi:10.5194/tcd-9-3741-2015.

Paull, C. K., W. Ussler III, S. R. Dallimore, S. M. Blasco, T. D. Lorenson, H. Melling, B. E. Medioli, F. M. Nixon, and F. A. McLaughlin (2007), Origin of pingo-like features on the Beaufort Sea shelf and their possible relationship to decomposing methane gas hydrates, *Geophys. Res. Lett.*, *34*, L01603, doi:10.1029/2006GL027977.

Paull, C. K., et al. (2011), Tracking the decomposition of submarine permafrost and gas hydrate under the shelf and slope of the Beaufort Sea, in *Proceedings of the 7th International Conference on Gas Hydrate*, 5581, 12, Edinburgh, U. K.

Portnov, A., A. J. Smith, J. Mienert, G. Cherkashov, P. Rekant, P. Semenov, P. Serov, and B. Vanshtein (2013), Offshore permafrost decay and massive seabed methane escape in water depths >20 m at the South Kara Sea shelf, *Geophys. Res. Lett.*, *40*, 3962–3967, doi:10.1002/grl.50735.

Portnov, A., J. Mienert, and P. Serov (2014), Modeling the evolution of climate-sensitive Arctic subsea permafrost in regions of extensive gas expulsion at the West Yamal Shelf, *J. Geophys. Res. Biogeosci.*, *119*, 2082–2094, doi:10.1002/2014JG002685.

Pullan, S., H. A. Macaulay, J. A. M. Hunter, R. L. Good, R. M. Gagne, and R. A. Burns (1987), Permafrost distribution determined from seismic refraction, *Geol. Surv. Can. Misc. Rep. 40*, 37 pp.

Rekant, P., G. Cherkashev, B. Vanstein, and P. Krinitsky (2005), Submarine permafrost in the nearshore zone of the southwestern Kara Sea, *Geo Mar. Lett.*, *25*(2-3), 183–189, doi:10.1007/S00367-004-0199-5.

Rogers, J., and J. Morack (1980), Geophysical evidence of shallow nearshore permafrost, Prudhoe Bay, Alaska, *J. Geophys. Res.*, *85*(B9), 4845–4853, doi:10.1029/JB085iB09p04845.

Romanovskii, N. N., A. V. Gavrilov, V. E. Tumskoy, A. L. Kholodov, C. Siegert, H.-W. Hubberton, and A. V. Sher (2000), Environmental evolution in the Laptev Sea region during late Pleistocene and Holocene, *Polarforschung*, *68*, 237–245.

Romanovsky, V. E., and T. E. Osterkamp (1996), Gas hydrate stability zone dynamics and global climate change, in *Global Glimpses Newsletter*, vol. 4, no. 2, Univ. of Alaska Fairbanks, Fairbanks. [Available at http://www.cgc.uaf.edu/newsletter/#gg4-2, last accessed Oct. 18, 2016.]

Ruppel, C. (2011), Methane hydrates and contemporary climate change, *Nat. Educ. Knowledge*, *2*(12), 12. [Available at http://www.nature.com/scitable/knowledge/library/methane-hydrates-and-contemporary-climate-change-24314790.]

Ruppel, C. D. (2015), Permafrost-associated gas hydrate: Is it really approximately 1% of the global system, *J. Chem. Eng. Data*, *60*(2), 429–436, doi:/10.1021/je500770m.

Ruppel, C. D., B. M. Herman, L. L. Brothers, and P. E. Hart (2016), Borehole Constraints on U.S. Beaufort Margin: 2. Borehole constraints, *Geochem. Geophys. Geosyst.*, *17*, doi:10:10.1002/2016GC006582.

Serov, P., A. Portnov, J. Mienert, P. Semenov, and P. Ilatovskya (2015), Methane release from pingo-like features across the South Kara Sea shelf, an area of thawing offshore permafrost, *J. Geophys. Res. Solid Earth*, *120*, 1515–1529, doi:10.1002/2015JF003467.

Shakhova, N., I. Semiletov, A. Salyuk, V. Yusupov, D. Kosmach, and O. Gustafsson (2010), Extensive methane venting to the atmosphere from sediments of the East Siberian Arctic Shelf, *Science*, *327*(5970), 1246–1250.

Sherwood, J. W. C. (1967), Refraction along an embedded high-speed layer, in *Seismic Refraction Prospecting*, edited by A. W. Musgrave, pp. 138–151, Soc. Explor. Geophys., Washington, D. C.

Taylor, A. E., S. R. Dallimore, P. R. Hill, D. R. Issler, S. Blasco, and F. Wright (2013), Numerical model of the geothermal regime on the Beaufort Shelf, arctic Canada since the Last Interglacial, *J. Geophys. Res. Solid Earth*, *118*, 2365–2379, doi:10.1002/2013JF002859.

Timur, A. (1968), Velocity of compressional waves in porous media at permafrost temperatures, *Geophysics*, *33*(4), 584–595.

Weingartner, T. J., S. R. Okkonen, and S. L. Danielson (2005), Circulation and water property variations in the nearshore Alaskan Beaufort Sea, *OCS Study MMS Rep. 2005-028*, 111 pp., Alaska OCS Region.

Zimmerman, R. W., and M. S. King (1986), The effect of the extent of freezing on seismic velocities in unconsolidated permafrost, *Geophysics*, *51*, 1285–1290.